

PREPRINT SUBMITTED NOT PEER-REVIEWED

This manuscript is a **preprint** uploaded to EarthArXiv. It has been **submitted** for publication to **GEOPHYSICAL RESEARCH LETTERS** on the **29/05/2025**. This preprint version of the manuscript has **not** undergone **peer-review**. Newer versions may be moderately different with slight variations in content. Authors encourage downloading the latest manuscript version from EarthArXiv before usage. Authors welcome feedback, discussion and comments anytime. For comments, you can use [hypothes.is](https://web.hypothes.is) (<https://web.hypothes.is/>).

Feel free to get in contact: geo.david.fernandez@gmail.com

Is the Suez Rift in its post-rift phase?

D. Fernández-Blanco^{1,2}, G. de Gelder³, and C. A-L. Jackson^{2,4}

¹*Geophysics and Resources Department, Institute of Deep-Sea Science and Engineering, Chinese Academy of Sciences, Sanya 57200, China*

²*Landscape and Basins Research Group (LBRG), Department of Earth Science and Engineering, Imperial College, London, SW7 2BP, UK*

³*ISTerre, CNRS, Université Grenoble Alpes, France*

⁴*WSP UK Ltd, 8 First St, Manchester, M15 4RP, UK*

Corresponding author: David Fernández-Blanco (geo.david.fernandez@gmail.com)

KEY POINTS

The Suez Rift shows pervasive normal faulting and Quaternary uplift after entering its presumed post-rift phase.

Footwall uplift rates up to 0.13 ± 0.04 mm/yr and extension rates up to 0.55 mm/yr indicate ongoing extension akin to the Basin and Range.

Active "post-rift" rifting challenges the binary classification of rifts as either active or failed in continental rift evolution.

KEYWORDS

Continental rifting

Active tectonics

Quaternary deformation

Geomorphic analysis

Failed rifts

ABSTRACT

Failed rifts are widely assumed to enter post-rift quiescence after termination of intracontinental rifting. This remains largely untested, however, and a comprehensive, regional evaluation of the rates and patterns of post-rift tectonic (in)activity is lacking. Our quantitative, rift-scale geomorphic study of the Suez Rift, an archetypal failed rift in Egypt, synthesizes isolated observations of faulting and coastal uplift, and reveals evidence for widespread “post-rift” rifting. Stacked topographic swaths and river profiles document pervasive normal fault offsets in Plio-Quaternary rocks along the rift length, with fluvial metrics showing steep gradients consistent with active and young faulting. Quaternary shorelines uplifted along both margins constrain normal fault footwall uplift rates of up to 0.13 ± 0.04 mm/yr, comparable to those of the Basin and Range, USA. This evidence of active extension in the Suez Rift, occurring after its presumed Pliocene failure, should motivate reevaluation of “failed” rifts and of conceptual models of continental rift evolution.

PLAIN LANGUAGE SUMMARY

The Suez Rift in Egypt has long been considered a “dead” or failed rift, an inactive trough in Earth's crust. Our research reveals the region is still actively being pulled apart. By studying the rift topography, raised ancient coral reefs and river patterns across the entire 300-km rift, we find ongoing faulting activity and associated vertical movement of the ground that raises the rift margins. Rates of extension are like those in the actively stretching Basin and Range. This unexpected activity challenges the traditional view that rifts simply “fail” and become inactive. Instead, the Suez Rift continues stretching at reduced rates despite most plate motion shifting elsewhere. Our findings suggest scientists need to reconsider how continental rifts evolve and that other supposedly “dead” rifts worldwide may also be more active than previously thought.

INTRODUCTION

Failed rifts are tectonically inactive intracontinental basins formed where lithospheric thinning by faulting halts before full oceanic spreading (Burke, 1977). Rifting fails due to changes in plate motion, mantle dynamics and/or preferential fault relocalization at triple junctions (Sengör and Burke, 1978). The subsequent post-rift phase of thermal subsidence leads to sedimentary infill of these elongated troughs during a period of tectonic quiescence sustained by regional force balance (Buiter et al., 2023; Brune et al., 2023).

The intracontinental Suez Rift, Egypt (Fig. 1) is thought to represent a key global example of a failed rift (Patton et al., 1994; Bosworth & McClay, 2001; Khalil & McClay, 2001; Moustafa & Khalil, 2020). Following extension and normal faulting in the Oligo-Miocene, the rift entered a phase of post-rift thermal subsidence and sedimentation, possibly in the Middle Miocene or earlier, when the Dead Sea Transform became the Nubian-Arabian plate boundary (Fig. 1A; Bartov et al., 1980; Steckler et al., 1988). This plate reorganization supposedly halted rifting in Suez except at its southern end, where extension and faulting persist near the junction between the Red Sea and Aqaba rifts (e.g., Bosworth and Taviani, 1996; Moustafa and Khalil, 2020).

Scattered geological observations and subtle geophysical signals suggest active tectonics also in the northern and central segments of the Suez Rift, challenging conventional views of post-rift tectonic quiescence. For example, Plio-Quaternary normal faulting and uplifted Quaternary shorelines document recent deformation (Andres and Radtke, 1988; Reyss et al., 1993; Choukri et al., 1995; Bosworth and Taviani, 1996), potentially driven by changes in the Euler pole between the Nubian and Arabian plates (Reilinger et al., 2006) and far-field stresses associated with establishment of the Afar plume (Ebinger et al., 2010). Widespread, low-magnitude

seismicity and GPS-derived crustal movements also support ongoing tectonic activity (Mahmoud et al., 2005; Badawy et al., 2008). This evidence is framed collectively as continued rift extension and late-rift subsidence across rift sub-basins (Bosworth and McClay, 2001, Bosworth et al., 2019). However, fragmentary spatial coverage and the absence of robust morphotectonic analyses hinders a coherent regional understanding, and a comprehensive evaluation of the span, patterns, and rates of the post-rift tectonic activity is needed.

Here, we present a quantitative, rift-scale analysis of post-rift tectonics in the Suez Rift (Fig. 1C). We integrate widely-tested geomorphic methods (Lajoie, 1986; Snyder et al., 2000), extended beyond their typical fault-scale, and novel quantitative displays of topography (Armijo et al. 2015; Fernández-Blanco, 2019) to examine the entire rift. Our analyses: (i) reveal pervasive normal faulting in Plio-Quaternary rocks, (ii) document tens of meters of Quaternary shoreline uplift along both margins, localized in the footwalls of crustal-scale, basin-bounding normal faults, and (iii) quantify tectonic activity along the entire rift length. Our quantitative evidence of extension in the putative post-rift phase challenges models of how continental rifts evolve and fail.

GEOLOGIC SETTING

The Suez Rift accommodated motion between the Arabian and Nubian plates north of the current intersection between the Red Sea Rift (Cochran, 1983) and the Aqaba Transform (Fig. 1A; Ribot et al., 2021). Magma-poor rifting from the Late Oligocene to Early Miocene created a 300-km-long, 80-km-wide basin, narrowing northwestward with decreasing extension, from Sinai's southern tip to Suez city (Fig. 1B; Patton et al., 1994).

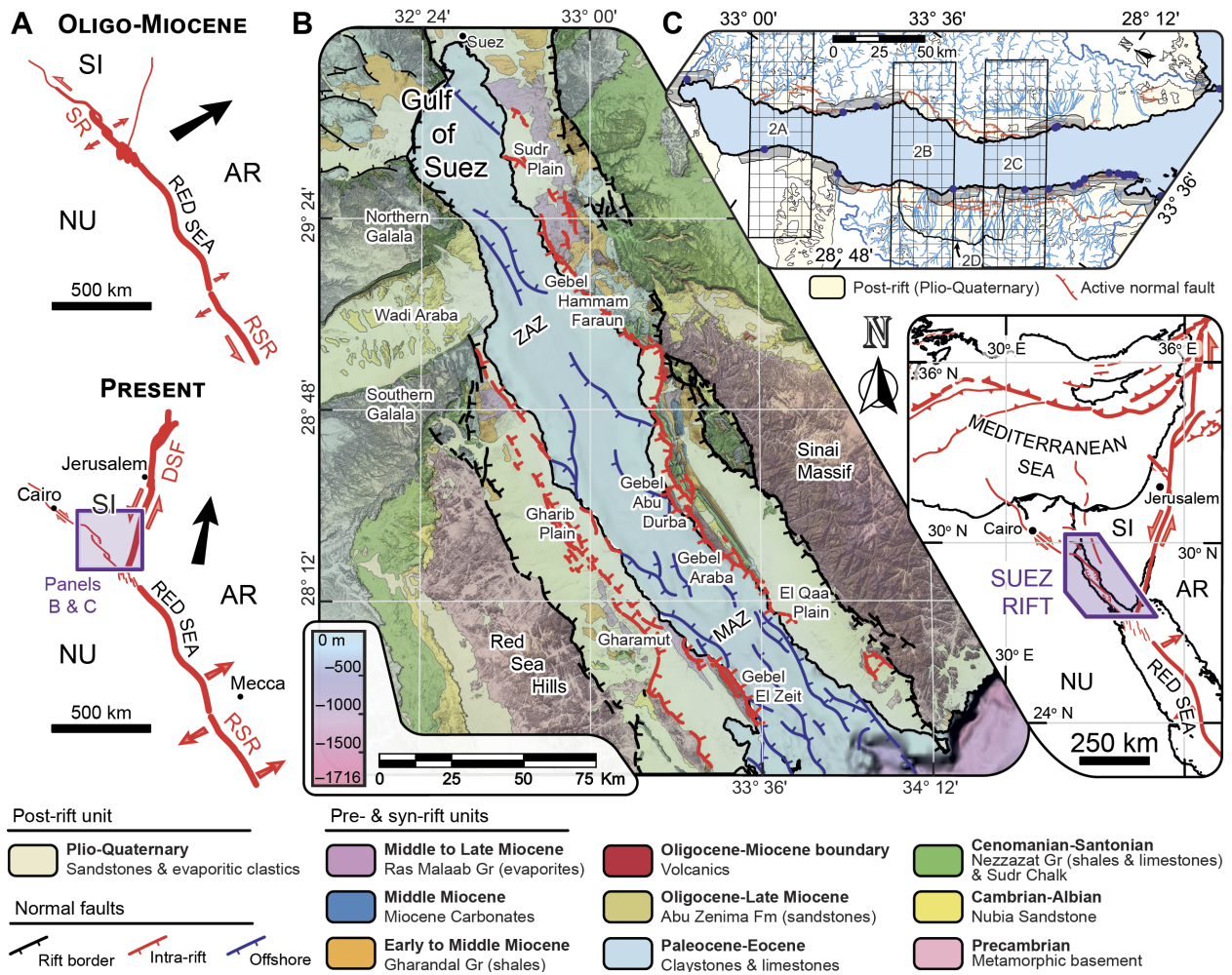


Figure 1. Tectonic frame, structural elements and stratigraphic units of the Suez Rift.

(A) Simplified plate boundary evolution in and around the Suez Rift since the Oligocene. Plates: SI-Sinai, AR-Arabia, NU-Nubia. Boundaries: SR-Suez Rift, RSR-Red Sea Ridge, AF-Aqaba Fault, DSF-Dead Sea Fault. (B) Geological and structural map showing main rift units and fault systems, overlaying EMODnet and ALOS DEM slope maps. Units and faults slightly modified from Moustafa and Khalil (2020). Newly-mapped and known intra-rift faults are in red. Text S1 details map sources, re-mapping criteria, and active fault mapping. Bottom right inset shows main plate boundaries and regional active structures. (C) Locations of geomorphic objects and subsequent figures. Georeferenced files are available in the GSA Data Repository for rift units (DR1), geologic units (DR2), faults (DR3), and river networks (DR4).

Intracontinental rifting led to three structural domains, with half-graben dip polarity alternating along the rift axis (Fig 1B; e.g., Moustafa, 1976; Moustafa and Khalil, 2020). Block-bounding, en-echelon faults are ~10-25 km long, strike predominantly rift-parallel (i.e., NW-SE) and accommodate throws of up to a few kilometers (Colletta et al., 1988; Moustafa and El-Raey, 1993).

METHODS

We use three robust and complementary geomorphic techniques to identify and quantify active tectonics across the entire Suez Rift (Fig. 1C): (i) hundreds of topographic swath profiles calculated from Digital Elevation Models (DEM) and stacked perpendicular to their trends, at rift-scale (300 swaths at ~100 m width, over ~30-km-wide, ~120-km-long stripes perpendicular to rift-bounding faults) and at rift margins (transecting post-rift rocks); (ii) Quaternary coral reef terraces compiled from 25 sites along both rift margins, corrected for eustatic and glacio-isostatic effects; and (iii) river and chi (χ) profiles, knickpoints and channel normalized steepness indices (k_{sn}) of the largest river networks on each rift margin, extracted from DEM data. Text S1 details datasets, the construction of the stacked swaths profiles, the compilation of coral reef terrace data, and the analyses of river networks.

ACTIVE RIFT-CONTROLLED RELIEF AND FAULTING

Relief across and along strike of the Suez Rift is highly asymmetric. The consistently shallow bathymetry (<50 m) of the rift along strike contrasts with its highly variable, rift-margin topography (Fig. 2, Fig. S1, Text S2). Inactive and still-active (see below) normal faults (black and red lines in Fig. 2A-C, respectively) bound major across-rift changes in topographic

gradient. Coastal mountains locally named *gebels* have asymmetric cross-rift topographies with steep, fault-bounded, gulf-facing escarpments (500 m of elevation change over ~2 km) and gentler, landward slopes (spanning over ~10 km) at Abu Durba-Araba, Hammam Faraum and El Zeit (Fig. 1, 2). Northward of these *gebels*, steep escarpments and surface displacements mark the base of triangular facets in Plio-Quaternary topography (red arrow heads in Fig. 2D).

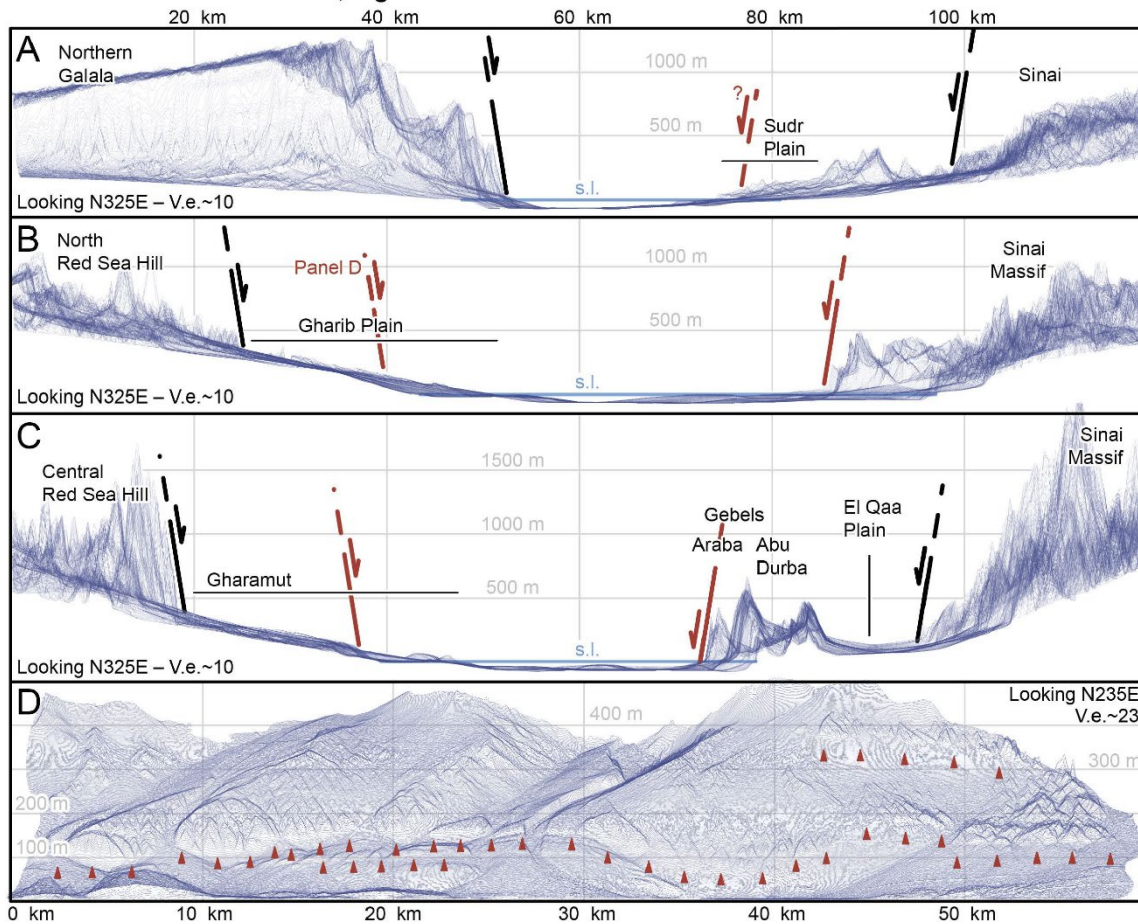


Figure 2. Suez Rift relief along its axis and two displays of coastal topography in Plio-Quaternary rocks. Axial topobathymetry of the rift in the Northern Galala (A), Northern Red Sea Hills (B), Central Red Sea Hills (C). Stacked swath profiles within 30-km-wide corridors (300 swaths at ~100 m width) viewed perpendicular to the controlling normal fault systems. (D) Stacked swath view (looking N235E, 300 swaths of ~100 m width) of the Gharib Plain perpendicular to the coast, from the sea landwards. Active faults are in red and inactive faults are in black.

QUATERNARY UPLIFT OF RIFT MARGINS

Raised Quaternary coral reef terraces at 25 sites record differential uplift along both margins across the entire rift (Fig. 3; Table S1). Some of these coral reef terraces were previously dated and correlated with Marine Isotope Stages (123.5 ± 8.5 ka, MIS 5e; 409 ± 16 ka, MIS 11c; see compilation by Bosworth et al., 2019). The maximum elevations of these terrace levels, 19 ± 0.5 m and 42 ± 1 m above sea level, occur at *gebel* centers, and allow us to calculate maximum uplift rates of 0.13 ± 0.04 mm/yr and 0.10 ± 0.2 mm/yr (Fig. 3B,D). MIS 5e terraces have comparable elevations at other *gebel* centers >200 km north of the rift's southern terminus yet are only a few meters above sea level at other sites (Fig. 3A; Gvirtzmann, 1994; Plaziat et al., 1998; Bosworth et al., 2019). At Gebel El Zeit, the most complete record of MIS 5e terraces reach a maximum elevation of $\sim 18.5 \pm 0.5$ m at the *gebel* center, and gradually decrease along the coast in both directions, reaching $\sim 6.5 \pm 0.5$ m at distances of ~ 40 km, defining a parabola of ~ 80 km length along the coastline (Fig. 3C). Two MIS 5e terraces at Gebel Hammam Faraum have comparable maximum elevation and along-strike elevation contrasts over similar horizontal distances (Fig. 3A).

PLIO-QUATERNARY DEFORMATION AND DRAINAGE DISEQUILIBRIUM

The disequilibrium of drainage networks provides evidence for and quantifies ongoing tectonics in Plio-Quaternary rocks on both rift margins (Fig. 4,S2,S3; DR4). On the western margin (Fig. 4C,4D), drainages 1-3 have rift-parallel gradients (normalized steepness indices from k_{sn} 0-25 to k_{sn} 50-75) and knickpoints where they cross small faults within the Plio-Quaternary unit.

Drainages 4-9 show peak normalized channel steepness values ($k_{sn} > 100$) that co-locate with river knickpoint clusters in Plio-Quaternary rocks, particularly along previously documented and

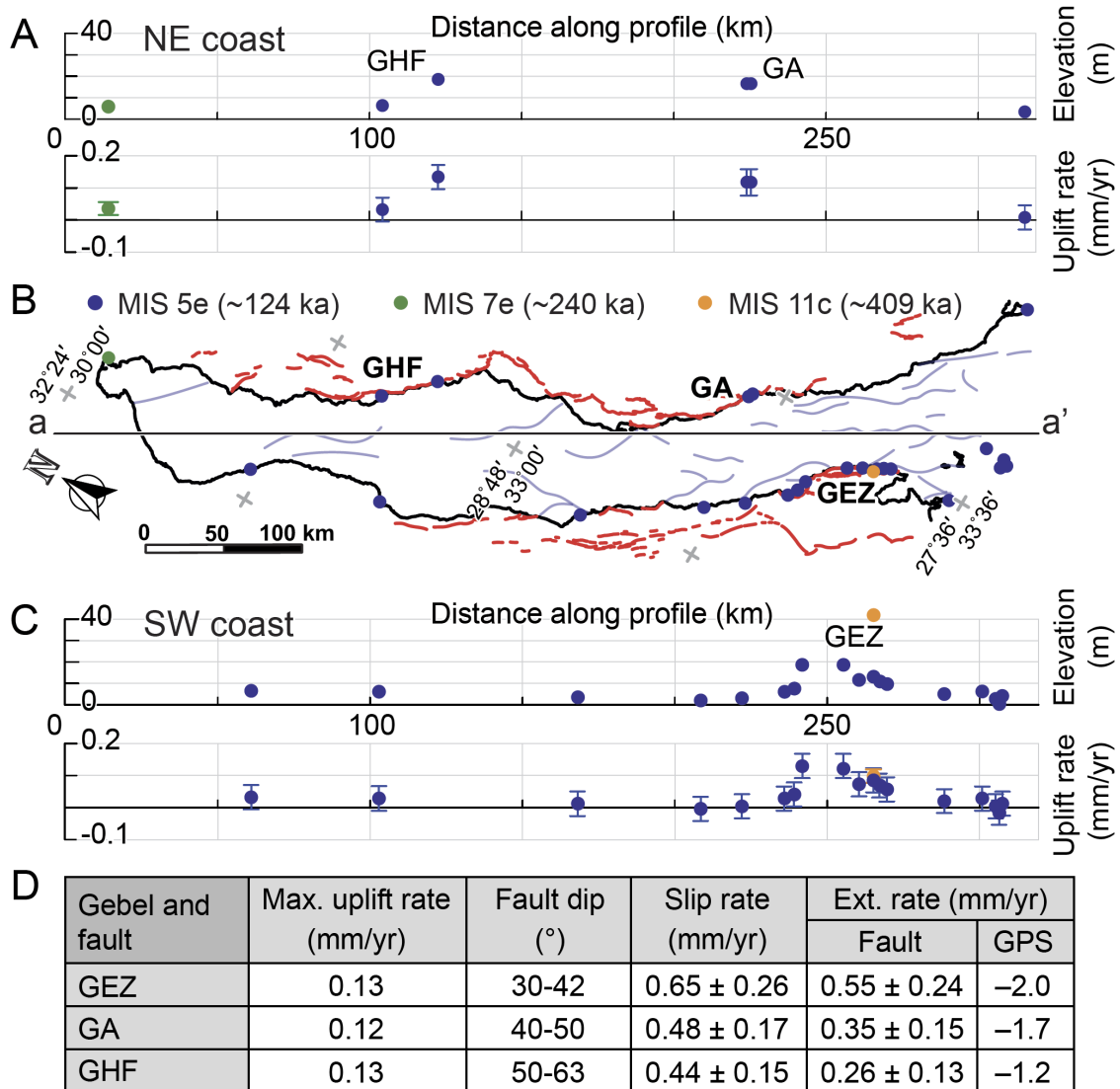


Figure 3. Quaternary coastal reef terraces in the Suez Rift margins. Terrace elevations in the (A) NE coast and (C) SW coast projected perpendicularly to profile a-a' (in the upper plot) and their calculated uplift rates with uncertainties (in the lower plot). (B) Map view of terrace locations and the location of profile a-a'. Colored dots indicate Marine Isotope Stages: MIS 5e (~123.5 ± 5.5, blue), MIS 7e (~240 ± 6 ka, green), and MIS 11c (~409 ± 16 ka, orange). (D) Calculated uplift, slip and extensional rates in main coastal faults. Key locations: GHF-Gebel Hammam Faraun, GA-Gebel Araba, GEZ-Gebel El Zeit. See Text S1 and Table S1 for details on sources, compilation criteria and rate calculations.

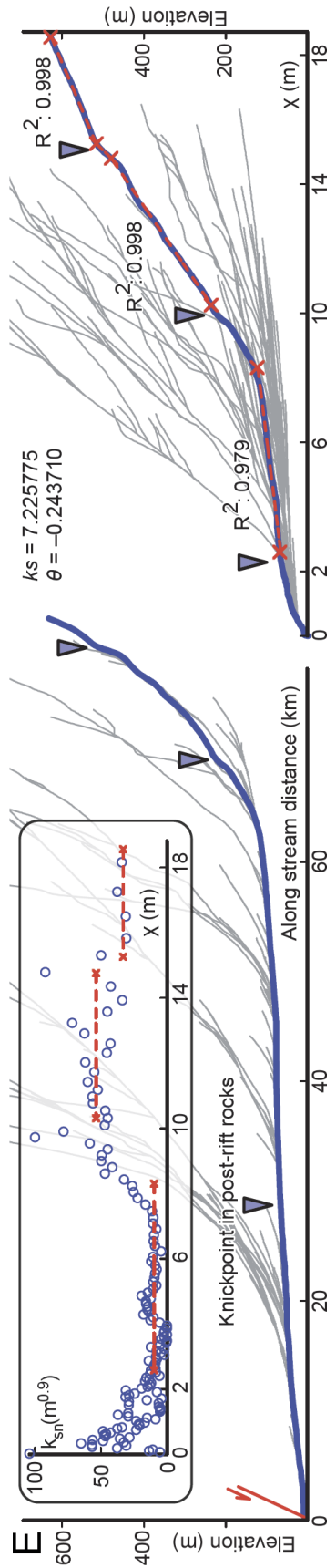
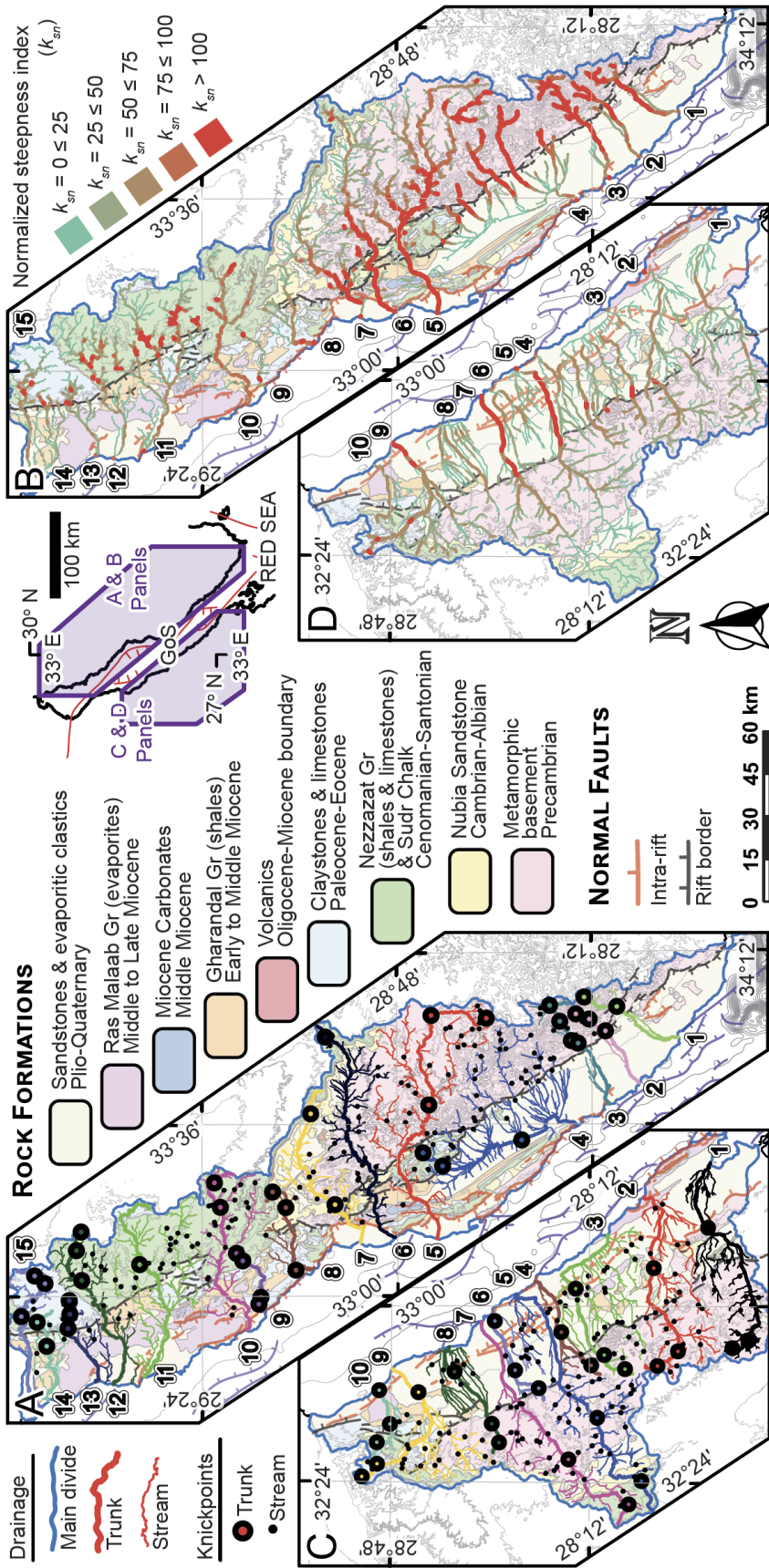


Figure 4. River catchments, tectonic knickpoints, and k_{sn} in rift margins, and two river channel profiles in Plio-Quaternary rocks. (A-C) Main drainages and knickpoints in the east and west margin, respectively. Trunk streams (thicker lines) and tributaries are colored by catchment and numbered south to north. Thicker colored dots mark trunk knickpoints; small black dots show tributary knickpoints. (B-D) Normalized steepness index (k_{sn}) maps for the east and west margin using reference concavity $\theta_{ref} = 0.45$. Colors range from green ($k_{sn} \leq 25$) to red ($k_{sn} > 100$). All panels overlay the geological map from Figure 1D. See larger versions of these maps in Fig. S2 and Fig. S3. (E) Displays of the longest river in the eastern margin (4, blue in the bottom half of panel, including longitudinal profile (left) and χ -elevation plot (right) of the trunk (thick blue) and some streams (gray). Trunk knickpoints are triangles and the one in Plio-Quaternary rocks is labeled. Inset shows k_{sn} variations with χ along the trunk. Complete analysis in DR4.

newly mapped, NW-SE-striking, basinward-dipping normal faults of small throw (Fig. 1C; Bosworth et al., 2020). On the eastern margin (Fig. 4A,B), drainages 1-3 have elevated normalized steepness indexes ($k_{sn} > 50$) throughout their linear profiles and anomalously high values for their drainage area ($k_{sn} > 100$) in streams draining Plio-Quaternary rocks. Drainages 4-7 are the largest and present peak normalized steepness index values ($k_{sn} > 100$) in Plio-Quaternary rocks. River 4 shows a knickpoint in Plio-Quaternary rocks and high k_{sn} values downstream of basement-bounding faults (Fig. 4E). Within Plio-Quaternary rocks, rivers 5-7 show consistently high normalized steepness channel values ($k_{sn} > 100$) from their outlet, whereas drainages 8-15 have linear profiles with $k_{sn} > 75$ near the coast.

EVIDENCE FOR “POST-RIFT” RIFTING

Evidence for recent and active normal faulting spans 250 km along strike of both rift margins, with normal fault networks uplifting and dissecting Plio-Quaternary rocks in the hanging walls of major rift-bounding faults at three structural locations; offshore (i.e. in the axis of the Gulf), along the coast, and within Plio-Quaternary rocks.

Offshore faults uplift coastal Plio-Quaternary plains. Although the activity of these faults is partially masked by sedimentation in the basin (Gawthorpe et al., 2003), the uplift of their footwalls results in river channels with elevated normalized steepness indexes (commonly with $k_{sn} > 50$; often with $k_{sn} > 100$) for their drainage area (e.g., Wobus et al., 2006).

Aside from knickpoints elevated in the rift topography, which may be pinned at threshold drainage areas (Crosby and Whipple, 2006), the consistent correlation of knickpoint locations with mapped faults across multiple drainage systems and across different stream orders (Fig. 4A,4C) support their tectonic origin, should the Plio-Quaternary rock strength be uniform. This evidence documents rift-wide active strain. Near-coast knickpoints that signal a transient adjustment to base-level changes and cannot be correlated by any mapped structure (Fig. 4E) likely result from offshore fault activity, although sea-level drop causes cannot be overruled.

Coastal faults produce *gebels*, distinctive, short-wavelength topographic asymmetries exposing syn- and pre-rift rocks (Fig. 2A-C). A ~80-km-long, MIS 5e parabola marks the footwall displacement profile of the gebel-bounding fault at El Zeit (Fig. 3C). Based on typical normal fault aspect ratios (Dawers et al., 1993), this length implies the bounding structure has a down-dip height of ~10-15 km and thus transects the seismogenic layer. Major instrumentally recorded earthquakes linked to this structure are indicative of active tectonic displacement (Jackson et al.,

1988; Huang and Solomon, 1987), and the consistent uplift rates between MIS 5e (0.13 ± 0.04 mm/yr) and MIS 11c (0.10 ± 0.2 mm/yr) support steady deformation since ~ 400 ka. We infer a comparable scale and pattern for the Gebel Hammam Faraum bounding fault, which has a similar terrace elevation contrasts over a comparable short horizontal distance (Fig. 3A), and accrued ~ 3 km of fault displacement after the late Middle Miocene (Gawthorpe et al., 2003). Assuming constant rates and negligible erosion, the maximum elevation of these gebels (~ 500 m) supports growth of their bounding faults since the Pliocene (3.12 ± 0.23 to 4.44 ± 0.2 Ma). This inferred timeframe aligns well with the localization of displacement along the fault and maximal accumulated offset in the late states of rifting, and its continued activity to date (Gawthorpe et al., 2003). Syntectonic deposits in the hanging walls of Gebel el Zeit and Hammam Faraum faults imply these faults were originally active during Aquitanian early rifting (e.g., el Atfy et al., 2013; Ramadan, 2014). The tectonic activity newly documented here therefore either represents reactivation or continued activity in these pre-existing faults.

“POST-RIFT” RIFTING RATES

Maximum footwall uplift rates at gebels (MIS 5e, 0.13 ± 0.04 mm/yr; MIS 11c, 0.10 ± 0.2 mm/yr) match those of slowly extending continental regions, like the Basin and Range, Usa (Ellis and Barnes, 2015) and the Rhine Graben Germany (Nivière et al., 2008), and exceed the hanging wall subsidence rates of 0.02 - 0.08 mm/yr (since 5 Ma or the Pliocene) documented for the Suez Rift (Moretti & Colletta, 1987). Given the lack of evidence for slip acceleration, this aligns well with regional uplift rates of ~ 0.05 mm/yr derived from geomorphic and stratigraphic markers across the rift flanks (Garfunkel, 1988). Together with the elevated uplift:subsidence ratios implied by flexural modeling, this supports lower-crustal and/or upper mantle viscosities (De Gelder et al., 2019). Using normal fault angles at *gebels*, reported to systematically decrease

southward from 63° to 30° (Jackson et al., 1988; Moustafa & Khalil, 2020), and empirically constrained uplift:subsidence ratios of $\sim 1:1-2.5$ from other intracontinental rifts (Basin and Range, King et al., 1988; Corinth Rift, De Gelder et al., 2019), we derive fault-normal slip rates of $\sim 0.44 \pm 0.15$ and $\sim 0.65 \pm 0.2$ mm/yr and rift-normal extension rates of $\sim 0.26 \pm 0.13$ to $\sim 0.55 \pm 0.24$ mm/yr (Fig. 3D). These extension rates are substantially lower than Oligocene rifting rates (2.0 mm/yr) and one-quarter to one-half of the Miocene rates (1.0 mm/yr) (Bosworth et al., 2005). They are also lower than the 0.8-1.2 mm/yr inferred at the same site and terrace level, MIS 5e (~ 125 kyr) at the Gebel el Zeit (direction 015° , NNE, Bosworth & Taviani, 1996). This discrepancy comes from their assumed coseismic uplift:subsidence ratio of 1:5-8, which may be appropriate for short-lived earthquake cycles but substantially exceeds the expected long-term range of 1:1-2.5 (King & Stein, 1988). Finally, our rates are about one-third of the 1.46 mm/yr oblique opening rate in a direction of 344° (NNW) between Sinai and Africa measured by GPS (Mahmoud et al., 2005; Bosworth & Durocher, 2017). However, our calculated rates are like the GPS-derived present-day rift-normal extension rate of 0.47 mm/yr, representing the Sinai-Africa velocity component perpendicular to the strike of the Gulf of Suez (Bosworth & Durocher, 2017 from Mahmoud et al., 2005).

Fault networks offsetting Plio-Quaternary rocks are documented at and northward of south Gharib Plain (Bosworth et al., 2019), and are here mapped also further north. Triangular facets mark these newly mapped faults (Fig. 1C; 2D). The systematic spatial correlation between their mapped traces, increased channel steepness and river knickpoints record their active, localized, differential vertical motion (Fig. 4A,C; Wobus et al., 2006).

POTENTIAL CAUSES FOR “POST-RIFT” RIFTING

Multiple potential causes may explain “post-rift” rifting in the Suez Rift. While sediment loading could enhance fault activity (e.g., De Sagazan and Olive, 2021), the lateral continuity of fault networks, their systematic dip variation, and the crustal-scale dimensions inferred from documented aspect ratios suggest deeper regional controls. GPS-derived extension rates ~3 times larger than our reported rates along an oblique direction to the rift (Mahmoud et al., 2005; Bosworth and Durocher, 2017; Fig. 3D) indicate significant off-fault strain and also support dominant regional thermal and plate boundary forces. The northwestward decrease in fault slip and extension rates could reflect a stress propagation gradient from the Afar plume (Ebinger et al., 2010). However, Mediterranean compression-driven, oblique slip (Badawy et al., 2008) and inherited structures, known to influence strain patterns in the northern Red Sea (Bosworth et al., 2019), could control local deformation in a more complex stress field. In contrast, strain localization along major faults is supported by our inferred elevated lower crustal viscosities, and a broadly coherent uplift and response along both margins suggest a dominant control by Nubian-Arabian plate motion changes (Reilinger et al., 2006).

IMPLICATIONS FOR INTRACONTINENTAL RIFT EVOLUTION

Active faulting during a period otherwise dominated by thermal subsidence in the Suez Rift challenges the simple binary "active" or "failed" classification typically applied to rifts. Our evidence expands the known spectrum of post-rift evolution margins (Buitter et al., 2022; Brune et al., 2023), documenting a lack of regional force balance expressed as significant tectonic activity after purported rift failure. Therefore, the Suez Rift does not fit its failed rift classification, for it continues to experience extension due to its proximity to an active plate

boundary. These findings suggest current models of continental rift evolution should be extended to explicitly account for failed rifts where tectonic activity persists despite the transferal of the main component of strain to adjacent or newly-formed deformation zones or plate boundaries, or elsewhere. A global reassessment of supposedly "failed" rifts is needed to capture the full spectrum of post-rift behavior and improve our understanding of continental rifting processes.

ACKNOWLEDGEMENTS

GdG acknowledges funding from the IRD and the Manajemen Talenta BRIN fellowship program, and research permit 52/SIP.EXT/IV/FR/5/2023 provided by the Indonesian government on May 11th 2023.

DATA AVAILABILITY STATEMENT

Data are available at: <https://figshare.com/s/9e0377dd79e734f34ad3>. This repository contains georeferenced datasets supporting our geomorphic analysis of active tectonics in the Suez Rift, Egypt. Files include:

- DR1: Rift units (georeferenced shapefile)
- DR2: Geological units (georeferenced shapefile)
- DR3: Fault maps including newly mapped active faults (georeferenced shapefile)
- DR4: River network analysis and drainage profiles

REFERENCE LIST

- Andres, W., Radtke, U., and Mangini, A., 1988, Quartäre Strandterrassen an der Küste des Gebel Zeit (Golf von Suez/Ägypten)(Quaternary Raised Beaches along the Gebel Zeit Coast (Gulf of Suez, Egypt)). *Erdkunde*, 7-16.
- Armijo, R., Lacassin, R., Coudurier-Curveur, A., and Carrizo, D., 2015, Coupled tectonic evolution of Andean orogeny and global climate: *Earth-Science Reviews*, v. 143, p. 1–35, <https://doi.org/10.1016/j.earscirev.2015.01.005>.
- Badawy, A., Mohamed, A.M.S., and Abu-Ali, N., 2008, Seismological and GPS constraints on Sinai sub-plate motion along the Suez rift: *Studia Geophysica et Geodaetica*, v. 52, p. 397–412, <https://doi.org/10.1007/s11200-008-0028-9>.
- Bartov, Y., Steinitz, G., Eyal, M., and Eyal, Y., 1980, Sinistral movement along the Gulf of Aqaba—its age and relation to the opening of the Red Sea: *Nature*, v. 285, p. 220–222, <https://doi.org/10.1038/285220a0>.
- Bosworth, W., and Taviani, M., 1996, Late Quaternary reorientation of stress field and extension direction in the southern Gulf of Suez, Egypt: Evidence from uplifted coral terraces, mesoscopic fault arrays, and borehole breakouts: *Tectonics*, v. 15, p. 791–802, <https://doi.org/10.1029/95TC03851>.
- Bosworth, W., and McClay, K., 2001, Structural and stratigraphic evolution of the Gulf of Suez rift, Egypt: a synthesis. In: Ziegler PA, Cavazza W, Robertson AHF, Crasquin-Soleau S (eds) Peri-Tethys Memoir 6: Peri-Tethyan Rift/Wrench basins and passive margins. *Mémoires du Muséum National d'Histoire Naturelle de Paris* 186:567–606
- Bosworth, W., Huchon, P., and McClay, K., 2005, The Red Sea and Gulf of Aden Basins: *Journal of African Earth Sciences*, v. 43, p. 334–378, <https://doi.org/10.1016/j.jafrearsci.2005.07.020>.
- Bosworth W, Durocher S (2017) Present-day stress fields of the Gulf of Suez (Egypt) based on exploratory well data: non-uniform regional extension and its relation to inherited structures and local plate motion. *J Afr Earth Sci*. <https://doi.org/10.1016/J.jafrearsci.2017.04.025>.

Bosworth, W., Taviani, M., and Rasul, N.M.A., 2019, Neotectonics of the Red Sea, Gulf of Suez and Gulf of Aqaba, in Rasul, N.M.A., and Stewart, I.C.F., eds., *Geological Setting, Palaeoenvironment and Archaeology of the Red Sea*: Cham, Springer International Publishing, p. 11–35, https://doi.org/10.1007/978-3-319-99408-6_2.

Bosworth, W., Khalil, S.M., Ligi, M., Stockli, D.F., and McClay, K.R., 2020, *Geology of Egypt: The Northern Red Sea*, in Hamimi, Z., El-Barkooky, A., Martínez Frías, J., Fritz, H., and Abd El-Rahman, Y., eds., *The Geology of Egypt*: Cham, Switzerland, Springer, *Regional Geology Reviews*, p. 243–374, https://doi.org/10.1007/978-3-030-15265-9_9.

Brune, S., Kolawole, F., Olive, J.-A., Stamps, D.S., Buck, W.R., Buitter, S.J.H., and Furman, T., 2023, *Geodynamics of continental rift initiation and evolution*: *Nature Reviews Earth & Environment*, v. 4, p. 235–253, <https://doi.org/10.1038/s43017-023-00391-3>.

Buitter, S.J.H., Brune, S., Keir, D., and Peron-Pinvidic, G., 2023, *Rifting continents*, in Duarte, J.C., ed., *Dynamics of Plate Tectonics and Mantle Convection*: Elsevier, p. 459–481, <https://doi.org/10.1016/B978-0-323-85733-8.00016-0>.

Burke, K., 1977, *Aulacogens and continental breakup*: *Annual Review of Earth and Planetary Sciences*, v. 5, p. 371–396, <https://doi.org/10.1146/annurev.ea.05.050177.002103>.

Choukri A, Reyss J-L, Plaziat J-C (1995) *Datations radiochimiques des hauts niveaux marins de la rive occidentale du Nord de la Mer Rouge au moyen de radioles d'oursin*. *C. R. Acad. Sci Paris* 321, série Iia:25–30

Cochran, J.R., 1983, *A model for development of Red Sea*: *AAPG Bulletin*, v. 67, p. 41–69, <https://doi.org/10.1306/03B5ACBE-16D1-11D7-8645000102C1865D>.

Colletta, B., Le Quellec, P., Letouzey, J., and Moretti, I., 1988, *Longitudinal evolution of the Suez Rift structure (Egypt)*: *Tectonophysics*, v. 153, p. 221–233.

Crosby, B. T., & Whipple, K. X. (2006). *Knickpoint initiation and distribution within fluvial networks: 236 waterfalls in the Waipaoa River, North Island, New Zealand*. *Geomorphology*, 82(1–2), 16–38. <https://doi.org/10.1016/j.geomorph.2005.08.023>.

Dawers, N.H., Anders, M.H., and Scholz, C.H., 1993, Growth of normal faults: Displacement-length scaling: *Geology*, v. 21, no. 12, p. 1107–1110, [https://doi.org/10.1130/0091-7613\(1993\)021<1107:GONFDL>2.3.CO;2](https://doi.org/10.1130/0091-7613(1993)021<1107:GONFDL>2.3.CO;2).

De Gelder, G., Fernández-Blanco, D., Melnick, D., Duclaux, G., Bell, R.E., Jara-Muñoz, J., and Strecker, M.R., 2019, Lithospheric flexure and rheology determined by climate cycle markers in the Corinth Rift: *Scientific Reports*, v. 9, 4260, <https://doi.org/10.1038/s41598-018-36377-1>.

De Sagazan, C., and Olive, J.-A., 2021, Assessing the impact of sedimentation on fault spacing at the Andaman Sea spreading center: *Geology*, v. 49, no. 4, p. 447–451, <https://doi.org/10.1130/G48263.1>.

Ebinger, C., Ayele, A., Keir, D., Rowland, J.V., Yirgu, G., Wright, T.J., Belachew, M., Hamling, I., and Campbell, E., 2010, Length and timescales of rift faulting and magma intrusion: The Afar rifting cycle from 2005 to present: *Annual Review of Earth and Planetary Sciences*, v. 38, p. 439–466, <https://doi.org/10.1146/annurev-earth-040809-152333>.

El Atfy, H., Brocke, R., & Uhl, D. (2013). Age and paleoenvironment of the Nukhul Formation, Gulf of Suez, Egypt: Insights from palynology, palynofacies and organic geochemistry. *GeoArabia*, 18(4), 137–174. <https://doi.org/10.2113/geoarabia.18.4.137>.

Ellis, M.A., and Barnes, J.B., 2015, A global perspective on the topographic response to fault growth: *Geosphere*, v. 11, no. 4, p. 1174–1190, <https://doi.org/10.1130/GES01156.1>.

Fernández-Blanco, D., de Gelder, G., Lacassin, R., & Armijo, R. (2019). A new crustal fault formed the modern Corinth Rift. *Earth-Science Reviews*, 199, 102919. <https://doi.org/10.1016/j.earscirev.2019.102919>.

Garfunkel, Z., 1988, Relation between continental rifting and uplifting: Evidence from the Suez rift and northern Red Sea: *Tectonophysics*, v. 150, no 1–2, p. 33–49, [https://doi.org/10.1016/0040-1951\(88\)90294-6](https://doi.org/10.1016/0040-1951(88)90294-6).

Gawthorpe, R.L., Jackson, C.A.-L., Young, M.J., Sharp, I.R., Moustafa, A.R., and Leppard, C.W., 2003, Normal fault growth, displacement localisation and the evolution of normal fault populations: the Hammam Faraun fault block, Suez rift, Egypt: *Journal of Structural Geology*, v. 25, no. 6, p. 883–895, [https://doi.org/10.1016/S0191-8141\(02\)00088-3](https://doi.org/10.1016/S0191-8141(02)00088-3).

Huang, P. Y., & Solomon, S. C. (1987). Centroid depths and mechanisms of mid-ocean ridge earthquakes in the Indian Ocean, Gulf of Aden, and Red Sea. *Journal of Geophysical Research: Solid Earth*, 92(B2), 1361-1382.

Jackson, J.A., White, N.J., Garfunkel, Z., and Anderson, H., 1988, Relations between normal-fault geometry, tilting and vertical motions in extensional terrains: An example from the southern Gulf of Suez: *Journal of Structural Geology*, v. 10, no. 2, p. 155–170, [https://doi.org/10.1016/0191-8141\(88\)90113-7](https://doi.org/10.1016/0191-8141(88)90113-7).

Khalil, S.M., and McClay, K.R., 2001, Tectonic evolution of the NW Red Sea-Gulf of Suez rift system.

King, G.C.P., Stein, R.S., and Rundle, J.B., 1988, The growth of geological structures by repeated earthquakes I. Conceptual framework: *Journal of Geophysical Research*, v. 93, p. 13,307–13,318, <https://doi.org/10.1029/JB093iB11p13307>.

Lajoie, K.R., 1986, Coastal tectonics, *in* Wallace, R.E., ed., *Active Tectonics*: Washington, D.C., National Academy Press, p. 95–124.

Mahmoud, S., Reilinger, R., McClusky, S., Vernant, P., and Tealeb, A., 2005, GPS evidence for northward motion of the Sinai Block: Implications for E. Mediterranean tectonics: *Earth and Planetary Science Letters*, v. 238, no. 1–2, p. 217–224, <https://doi.org/10.1016/j.epsl.2005.06.063>.

Moretti, I., and Colletta, B., 1987, Spatial and temporal evolution of the Suez rift subsidence: *Journal of Geodynamics*, v. 7, no. 1–2, p. 151–168, [https://doi.org/10.1016/0264-3707\(87\)90069-X](https://doi.org/10.1016/0264-3707(87)90069-X).

Moustafa, A.M. (1976). Block faulting in the Gulf of Suez. In *Proceedings of the 5th Egyptian General Petroleum Corporation Exploration Seminar (Vol. 35)*.

Moustafa, A.R., and El-Raey, A.K., 1993, Structural characteristics of the Suez rift margins: *Geologische Rundschau*, v. 82, p. 101–109, <https://doi.org/10.1007/BF00563273>.

Moustafa, A.R., and Khalil, S.M., 2020, Structural Setting and Tectonic Evolution of the Gulf of Suez, NW Red Sea and Gulf of Aqaba Rift Systems, in Hamimi, Z., El-Barkooky, A., Martínez Frías, J., Fritz, H., and Abd El-Rahman, Y., eds., *The Geology of Egypt: Cham, Springer, Regional Geology Reviews*, p. 295–342,

https://doi.org/10.1007/978-3-030-15265-9_8.

Patton, T.L., Moustafa, A.R., Nelson, R.A., and Abdine, S., 1994, Tectonic evolution and structural setting of the Suez Rift: Chapter 1: Part I. Type Basin: Gulf of Suez, in Landon, S.M., ed., *Interior Rift Basins: American Association of Petroleum Geologists Memoir 59*, p. 9–55.

Ramadan, F. S. (2014). The Nature of Pre-Miocene and Miocene Sediments in the Offshore Northern Part of the Gulf of Suez, Egypt. *Petroleum science and technology*, 32(10), 1241-1256.

Reyss JL, Choukri A, Plaziat JC, Purser BH (1993) Datations radiochimiques des récifs coralliens de la rive occidentale du Nord de la Mer Rouge, premières implications stratigraphiques et tectoniques. *C. R. AcadSci Paris 317, série II*:487–492

Nivière, B., Bruestle, A., Bertrand, G., Carretier, S., Behrmann, J., and Gourry, J.C., 2008, Active tectonics of the southeastern Upper Rhine graben, Freiburg area (Germany): *Quaternary Science Reviews*, v. 27, p. 541–555, <https://doi.org/10.1016/j.quascirev.2007.11.018>.

Reilinger, R., et al., 2006, GPS constraints on continental deformation in the Africa-Arabia-Eurasia continental collision zone and implications for the dynamics of plate interactions: *Journal of Geophysical Research: Solid Earth*, v. 111, B05411, <https://doi.org/10.1029/2005JB004051>.

Ribot, M., Klinger, Y., Jónsson, S., Avsar, U., Pons-Branchu, E., Matrau, R., and Mallon, F.L., 2021, Active faults' geometry in the Gulf of Aqaba, southern Dead Sea Fault, illuminated by multibeam bathymetric data: *Tectonics*, v. 40, e2020TC006443, <https://doi.org/10.1029/2020TC006443>.

Sengör, A.C., and Burke, K., 1978, Relative timing of rifting and volcanism on Earth and its tectonic implications: *Geophysical Research Letters*, v. 5, p. 419–421, <https://doi.org/10.1029/GL005i006p00419>.

Snyder, N.P., Whipple, K.X., Tucker, G.E., and Merritts, D.J., 2000, Landscape response to tectonic forcing: Digital elevation model analysis of stream profiles in the Mendocino triple junction region, northern California: GSA Bulletin, v. 112, no. 8, p. 1250–1263, [https://doi.org/10.1130/0016-7606\(2000\)112<1250:LRTTFD>2.0.CO;2](https://doi.org/10.1130/0016-7606(2000)112<1250:LRTTFD>2.0.CO;2).

Steckler, M.S., Berthelot, F., Lyberis, N., and Le Pichon, X., 1988, Subsidence in the Gulf of Suez: Implications for rifting and plate kinematics: Tectonophysics, v. 153, no. 1–4, p. 249–270, [https://doi.org/10.1016/0040-1951\(88\)90019-4](https://doi.org/10.1016/0040-1951(88)90019-4).

Wobus, C., Whipple, K.X., Kirby, E., Snyder, N., Johnson, J., Spyropolou, K., Crosby, B., and Sheehan, D., 2006, Tectonics from topography: Procedures, promise, and pitfalls: Geological Society of America Special Papers, v. 398, p. 55–74, [https://doi.org/10.1130/2006.2398\(04\)](https://doi.org/10.1130/2006.2398(04)).